Substrate, focal adhesions, and actin filaments: a mechanical unit with a weak spot for mechanosensitive proteins

2010 J. Phys.: Condens. Matter 22 194109

(http://iopscience.iop.org/0953-8984/22/19/194109)

J. Phys.: Condens. Matter **22** (2010) 194109 (10pp) doi:10.1088/0953-8984/22/19/194109

Substrate, focal adhesions, and actin filaments: a mechanical unit with a weak spot for mechanosensitive proteins

David Kirchenbüchler, Simone Born, Norbert Kirchgeßner, Sebastian Houben, Bernd Hoffmann[1] and Rudolf Merkel

Institute of Bio- and Nanosystems, IBN-4, Biomechanics, Research Centre Jülich GmbH, 52425 Jülich, Germany

E-mail: b.hoffmann@fz-juelich.de

Received 16 September 2009, in final form 18 November 2009
Published 26 April 2010
Online at stacks.iop.org/JPhysCM/22/194109

Abstract

Mechanosensing is a vital prerequisite for dynamic remodeling of focal adhesions and cytoskeletal structures upon substrate deformation. For example, tissue formation, directed cell orientation or cell differentiation are regulated by such mechanosensing processes. Focal adhesions and the actin cytoskeleton are believed to be involved in these processes, but where mechanosensing molecules are located and how elastic substrate, focal adhesions and the cytoskeleton couple with each other upon substrate deformation still remains obscure. To approach these questions we have developed a sensitive method to apply defined spatially decaying deformation fields to cells cultivated on ultrasoft elastic substrates and to accurately quantify the resulting displacements of the actin cytoskeleton, focal adhesions, as well as the substrate. Displacement fields were recorded in live cell microscopy by tracking either signals from fluorescent proteins or marker particles in the substrate. As model cell type we used myofibroblasts. These cells are characterized by highly stable adhesion and force generating structures but are still able to detect mechanical signals with high sensitivity. We found a rigid connection between substrate and focal adhesions. Furthermore, stress fibers were found to be barely extendable almost over their whole lengths. Plastic deformation took place only at the very ends of actin filaments close to focal adhesions. As a result, this area became elongated without extension of existing actin filaments by polymerization. Both ends of the stress fibers were mechanically coupled with detectable plastic deformations on either site. Interestingly, traction force dependent substrate deformation fields remained mostly unaffected even when stress fiber elongations were released. These data argue for a location of mechanosensing proteins at the ends of actin stress fibers and describe, except for these domains, the whole system to be relatively rigid for tensile strain with a mechanical coupling between the front and rear end of a cell.

1. Introduction

Cellular mechanics of sessile cells faces a fascinating conflict of constructing on the one hand a preferably stiff force transmission system for efficient transfer of generated forces to the outer environment. On the other hand the same system needs to be highly sensitive to outer mechanical signals to enable a cellular mechanoresponse. These processes can include small morphological changes, as described for many cell types upon cyclic stretch application with cytoskeletal and cell shape reorientations perpendicular to the direction of stretch [1, 2]. Functional adaptations such as strengthening adhesion sites or stress fibers upon mechanical loading [3–7], and even complete differentiation processes of precursor cells [8, 9] or stem cells [10] e.g. upon elasticity recognition, are mentioned just as further examples.

[1] Author to whom any correspondence should be addressed.

The mechanical system of sessile cells essential for traction force generation and transmission is relatively well understood [11, 12]. Bundles of actin filaments are connected by various types of cross-linker proteins, such as e.g. α-actinin, to form stress fibers spanning parts or even the whole length of a cell [13]. Within these stress fibers myosin II molecular motor proteins are incorporated. Upon activation, these motor proteins undergo permanent cycles of conformational changes to slide actin filaments against each other, resulting in a contraction of the stress fiber [14]. At the same time, stress fiber ends are connected with the outer environment by complexes called focal adhesions (FAs). These sites bind to extracellular matrix molecules via integrin molecules and attach stress fiber ends to integrins by a large number of intracellular FA proteins [15]. Up to now more than 100 proteins have been described to be at least temporarily involved in FA composition. Due to this connection, stress fiber generated traction forces are transferred to the extracellular environment. These traction forces are vital for almost every cell for e.g. intracellular organization, morphology, generation of tissue tension or motility [16–18].

Compared to the force generation and transition system much less is known about recognition, as well as transduction, of extracellular mechanical signals applied to cells. A constantly increasing body of literature is indicating that mechanical signals as shear flow [19], elasticity [9, 20–22], strain [23] and topography [24–27] are universally recognized by cells. Unfortunately, how these signals are sensed, and whether different mechanical signals are detected by independent or interwoven signal cascades, is still largely unknown. Several hypotheses are discussed. Strain sensitive ion channels, presentations of hidden sequences upon stretch of the extracellular matrix molecule fibronectin or formation of force-stabilized receptor–ligand bonds (catch bonds) are possible mechanisms [28–31]. These systems could work in parallel to a stretch insensitive force generation and transition apparatus. Challenging is that stretch sensitive ion channels such as TRPM7 [32] are possibly not overall expressed in mammalian cells. Also hidden sequences within matrix molecules are at least not the only mechanism of how cells are able to recognize mechanical signals, since mechanical responses are largely independent of substrate coatings used in cell culture. A model of possibly identical importance combines force generation/transition and recognition of mechanical signals in one and the same system [33–35]. Here, mechanosensitive molecules are incorporated into the actin filament/focal adhesion apparatus. Mechanical signals lead to a modified tension within the system, resulting in conformational changes within mechanosensors and, therefore, in their activation or inactivation. An interesting candidate for a mechanosensoric protein is e.g. p130Cas [36]. p130Cas is composed of three subdomains of which the N-terminal as well as the C-terminal domain localize the protein in FAs while the inner domain consists of a repetitive number of putative tyrosine phosphorylation motifs. *In vitro* experiments could show enhanced phosphorylation levels upon extension of p130Cas, which in turn were assumed to activate Crk/C3G-Rap1 signaling. A mechanosensoric mechanism on a similar level is also discussed for the adhesion site as well as actin binding proteins α-actinin and zyxin [37, 38]. Here, tension in actin stress fibers was proposed to induce a conformational elongation in α-actinin, which in turn could increase the accessibility of zyxin binding sites.

All models based on structural unfolding of protein conformations upon mechanical loading fully depend on domains within the stress fiber/FA system that are sensitive to stretch. Localization of mechanosensor proteins in areas behaving stiffly, and therefore lacking elongation upon stretch, would lead to a loss of signal recognition. First experiments indicate that stress fibers act under tension like stiff cables due to incorporated molecular motors [39]. Interestingly, the same motors induce immediate contraction of stress fibers as soon as the connection between stress fibers and FAs is weakened [40, 41]. How stable FAs are affected by force application is largely unknown. Growth and strengthening processes have been observed only on young FAs while mature FAs are largely unaffected by identical signals [4–6]. Furthermore, FAs of motile cells, and therefore characterized by enhanced actin retrograde flow, were deformed in the direction of the stress fibers [42]. Whether this finding also holds for sessile cells, with their structurally stabilized adhesion structures, remains unclear.

In this work we therefore focused on mechanical characterization of the stress fiber/FA system of stably adhered cells upon application of spatially decaying substrate deformation fields. Simultaneous analysis of substrate, FAs and stress fiber displacements allowed us to pinpoint the spot most sensitive to stretch, down to the ends of stress fibers. These ends are plastically deformed upon single substrate stretch. Simultaneous substrate deformation field analysis additionally indicates that mechanosensation, via protein elongation, can occur without significantly affecting transmitted traction forces.

2. Material and methods

2.1. Cell isolation and culture conditions

Cardiac fibroblasts were isolated from 19-day-old Wistar rat embryos. In brief, pregnant rats were anesthetized with CO_2 and decapitated. Embryos were removed and decapitated under sterile conditions. The hearts were quickly isolated, and washed two times with Hank's balanced salt solution (HBSS, Lonza). The hearts were cut into small pieces and digested one time in a 0.5% trypsin 0.2% EDTA solution in HBSS at 37 °C (TE, Sigma). The supernatant was discarded and the remaining pieces were incubated with 1000 units DNase (DNase II type V, Sigma). Pieces were digested by TE a second time and separated cells were collected by centrifugation at 200 g for 10 min.

Cells were cultured *in vitro* under standard culture conditions (37 °C, 5% CO_2). As a culture medium F10 Ham's was used supplemented with 10% fetal bovine serum, a 1:100 dilution of an antibiotic solution (10 000 units penicillin and 10 mg ml^{-1} streptomycin in 0.9% NaCl, Sigma) and a 1:200 dilution of a solution containing insulin (1 mg ml^{-1}),

transferrin (0.55 mg ml^{-1}), and sodium selenite (0.5 μg ml^{-1}) (Sigma). For differentiation of cardiac fibroblasts to myofibroblasts, cells were cultured in plastic dishes (6 cm, Nunc) for 4 days.

2.2. Plasmid constructs and transfection

Where necessary, cells were transfected by nucleofection (Amaxa GmbH, Cologne, Germany). 3×10^5 cells were detached by trypsinization and resuspended in Amaxa solution together with 3 μg of plasmid-DNA. The eGFP-Vinculin construct used here was kindly provided by B Geiger (Weizmann Institute of Science, Rehovot, Israel). GFP-VASP was a gift from Jürgen Wehland (University Braunschweig, Germany). The plasmid pEGFP-Actin was purchased from BD-Biosciences (Heidelberg, Germany). Open reading frame of p130CAS cDNA (NCBI: BC062556) was cloned into pEGFP-C1 (Clontech, Saint-Germain-en-Laye, France) resulting in clone BH371. An open reading frame of VASP cDNA (NCBI: BC038224) was cloned into pDsRed-Monomer-C1 (Clontech), resulting in clone BH378. Immediately after nucleofection (Nucleofektor [programm G-09]), 7000–40 000 cells were transferred to silicone rubber substrates coated with 5 μg cm^{-2} fibronectin. Cells were analyzed from day 2 to 5 after transfection.

2.3. Preparation of elastomeric silicone rubber substrates

Preparation of bead micropatterned elastomeric substrates was performed as described in [43]. In brief, as source material, a two-component silicone rubber (PDMS) formulation (Sylgard 184, Dow Corning, Wiesbaden, Germany) consisting of base material and cross-linker was used. The substrates used here were fabricated using base and cross-linker at a mixing ratio of 50:1 (w/w). The material properties of the resulting cross-linked rubbers were determined as described before [44] giving a Poisson's ratio of 0.5 and a Young's modulus of 16 kPa. For micropatterning, fluorescent FluoSpheres (0.2 μm, Crimson, Invitrogen, Karlsruhe, Germany) were used in the top layer (below 1 μm thickness) of the substrates. Cross-linking of silicone rubber was performed at 60 °C overnight. Elastomeric substrates were glued to the bottom of 3.5 cm Petri dishes to cover predrilled 1.5 cm holes.

2.4. Application of decaying deformation fields

To induce decaying deformation fields in silicone rubber we used the tip of a gauge needle (Neolus ⌀0.7 mm, Terumo, Eschborn, Germany) mounted to a micromanipulator (MHW-3, Narishige, Tokyo, Japan). The tip was placed at approximately 40 μm distance from a selected cell. It was poked 4 μm into the substrate and decaying deformation fields were induced stepwise by moving the tip sideways. A complete deformation cycle typically consisted of 5–10 steps, each with a tip displacement of 1 μm. Time intervals between two consecutive displacement steps were in the range of 10–20 s. For some experiments the relaxation of decaying deformation fields was accelerated by returning the tip to the original position before removal of the needle from the rubber. Time series of all analyzed cells were captured spanning the complete time from 100 s before needle insertion to 200 s after the whole deformation cycle.

2.5. Light microscopy

Living cells were analyzed using a confocal microscope (LSM510 Meta, Carl Zeiss, Jena) equipped with a 63 × 1.4 NA PlanApochromat oil objective (Carl Zeiss). Cells were maintained at 37 °C. eGFP was excited with the 488 nm line of an argon ion laser and detected using a 505-530 band pass filter. Fluorescent beads or DsRed constructs were excited by the 543 nm line of a green helium–neon laser. For detection we used a 650 nm (fluorescent beads) or 580 nm (DsRed constructs) long pass filter, respectively.

The regions of interest to be bleached of GFP constructs were selected using the LSM 510 software V.3.2 SP2 software tool (Carl Zeiss, Jena). ROIs were bleached at 488 nm at full intensity for 40 μs per pixel (0.0081 μm^2/pixel). Bleached areas were detectable for more than 10 min i.e. throughout the whole subsequent analysis time.

2.6. Image processing

All image processing was performed using MATLAB (7.8 R2009a, MathWorks, Natick, MA, USA). To reduce the effect of intensity noise, all images were prefiltered with a 5 × 5 normalized binomial filter. Since convolution with a binomial mask has translational symmetry, small objects such as shot noise are removed, whereas objects of larger size remain intact and unshifted, and can thus be tracked with enhanced subpixel accuracy by cross-correlation. The positions of fluorescently labeled structures in the cell were analyzed versus the underlying substrate upon substrate deformation. Structure positions were marked manually in the first image of a time series spanning the whole manipulation cycle. For actin we tracked the edges of bleached regions. For FA analysis only defined bright adhesions were selected. For image processing marked positions were used as centers of templates spanning the whole focal adhesion or the entire bleached edge. Every template was now tracked over time by cross-correlation. The computational time was minimized by restricting the search areas to rectangles around the previous positions. To compare the actin and FA displacements with the one of the underlying substrate, the marked positions of GFP signals in the first image were also used as centers of a template showing the substrate embedded fluorescent beads to be tracked simultaneously. Thus, fluorescent beads directly below, or closely around, these spots were taken as the new template and subsequently tracked over time, as described above.

For time–space analyses, intensity profiles of rectangular areas were calculated. Areas were oriented along FAs and stress fibers, and therefore perpendicular to bleach lines. Areas were 10 pixels (i.e. 0.9 μm) wide and intensities were averaged over their width. Any structures of interest were marked by hand and tracked in 1D by cross-correlation, as mentioned before.

2.7. Displacement field measurements of cells

Cells were grown on bead micropatterned, elastomeric substrates. The substrate deformations caused by cells were analyzed by measuring the displacements of fluorescent bead, as described in [43], before and after induction of external decaying deformation fields. In brief, bead positions in the first image were determined with a pattern function generated from a manually chosen bead. Small areas around each position were used in the later steps as templates. The position of every template was tracked by cross-correlation, as described before. For every time step all bead positions were corrected for the lateral drift from the picture. The lateral drift was determined by the average shift of beads far away from the cell. To get a reference image of fluorescent beads without the cell, cells were detached from the substrate by scraping them off with the needle. Complete removal was confirmed by complete loss of the GFP-signal. For mean displacement analysis we selected, in the first image (i.e. before substrate deformation), those 50% of beads exhibiting the highest displacement. Only these beads were tracked to exclude parts of the images unaffected by the cell. From the displacements of these beads we calculated the mean substrate displacement caused by the cell before and after the stretch.

3. Results

3.1. Focal adhesions follow substrate deformation

The cellular environment, the focal adhesions (FAs) of a cell, as well as its actin cytoskeleton, form a mechanical unit which is essential for generation and transmission of forces and vital for recognition and processing of external mechanical signals. In order to probe the elasticity and cohesion strength of the linkages between these individual components, we applied well defined, spatially decaying deformation fields to myofibroblasts grown on micropatterned elastomeric substrates mimicking the cellular environment (figure 1). Substrate deformation fields were induced in front of myofibroblasts with sufficient distance to the cell. Displacement field strength, i.e. needle translation was adjusted to reach substrate displacement values close to the detection limit between the cell's center and the side of the cell opposed to the needle.

In order to determine the spatial displacement of FAs upon substrate deformation, myofibroblasts were transfected with GFP-VASP (figure 2(A)). The cytoskeletal/FA apparatus of myofibroblasts was spatially stable over hours (data not shown). This was a prerequisite for all analyses performed here. Induced substrate deformations were kept low (1–3% total cell elongation) to mimic natural conditions and to prevent cell damage. GFP-VASP and underlying substrate beads were tracked over time (figure 2(B)). Comparing bead displacements with those of VASP-labeled FAs revealed identical displacement values for every adhesion site in the decaying deformation field no matter whether the adhesion was close to or far from the microneedle ($n = 122$ adhesions of 10 cells, figure 2(C)). Identical results were observed for FAs labeled with GFP versions of vinculin ($n = 101$ FAs of 7 cells), α-actinin ($n = 26$ FAs of 3 cells) and even p130Cas ($n = 33$ FAs of 4 cells) (data not shown), arguing for a very rigid connection between the substrate and FAs as a whole.

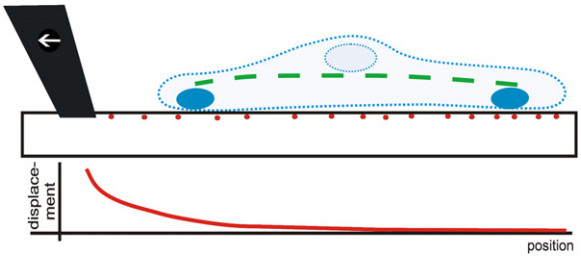

Figure 1. Cells in decaying deformation fields. Myofibroblasts were incubated on fibronectin coated, soft silicone rubber substrates. Fluorescent beads were embedded into the top substrate layer (red dots). Using a microneedle (black) a spatially decaying deformation field (red curve) was applied to the substrate. Deformation fields were adjusted to reach the detection limit below the center of the cell, resulting in total cell elongations of 1–3% and decaying substrate deformation. Blue circle = FAs, dashed green line = actin stress fiber.

3.2. The inner part of actin stress fibers is barely extendable

Since all analyzed FA proteins displaced exactly with the substrate, in the next step we analyzed the displacements and deformations of GFP-actin labeled stress fibers of cells in a decaying substrate deformation field ($n = 10$ stress fibers of 8 independent cells). To characterize stress fiber elasticities, several consecutive lines perpendicular to the main filament orientation were bleached into the fibers (figure 3(A)). The resulting sharp gray-value edges enabled us to track stress fiber displacement relative to the displacement of the substrate below the fiber for the main part of the fiber (figures 3(B) and C). Only the ends of stress fibers were not tracked due to their faint and diffuse image. We focused on isolated actin stress fibers at cell borders. This was important for accurate and clear-cut mechanical characterization of single fibers since connections to surrounding actin bundles or branching of stress fibers needed to be minimized. Measurement of bead displacements at maximal substrate deformation confirmed the spatial decay of the substrate deformation field (figure 4). In contrast, displacements of points along actin stress fibers exhibited a much weaker, approximately linear decay. The displacement values were in between the maximal and minimal substrate deformation below the stress fiber (figure 4). In order to quantify the slope of the decay, the slope of an ideal spring rigidly connected to the substrate only at its ends was used as reference, i.e. it was set to 100%. Such a spring would show a decay given by a straight line between the substrate beads directly located below the stress fiber ends. The other extreme, a slope of 0%, corresponds to a rigid, inextensible rod. We found that the slope of the stress fiber decay amounted on average to just 12% of the value expected for a spring rigidly connected to both FAs. The highest value observed amounted to 50%. These data prove stress fibers to be relatively rigid upon tensile strain and also show that the entire substrate/FA displacement is not transduced into actin filaments.

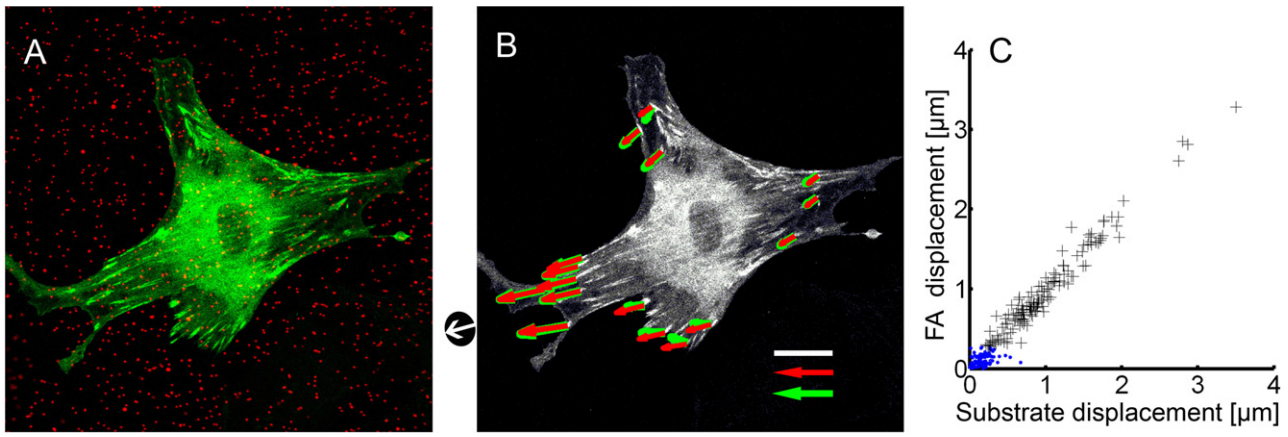

Figure 2. FAs follow substrate deformation. (A) Myofibroblasts were transfected with GFP-VASP and grown for two days on bead micropatterned PDMS substrates. (B) Near the left side of the cell a decaying deformation field was applied to the substrate using a microneedle (black dot). Its translation is indicated by the white arrow. The resulting displacements of VASP-labeled FAs (green arrows) were analyzed at maximum substrate deformation and compared to the displacement of substrate beads directly below the FAs (red arrows). Scale bar = 20 μm, scale arrows = 2 μm displacement. (C) Substrate displacement versus FA displacement before (blue dots) and at maximum substrate deformation (black crosses). $n = 122$ FAs from 10 independent experiments. Note that coinciding displacement values for FA proteins and underlying substrate beads were also found for α-actinin, vinculin and p130Cas.

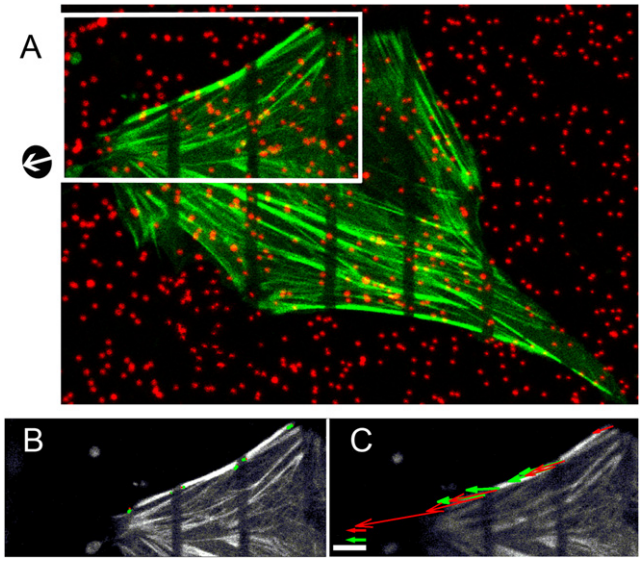

Figure 3. Mechanically stretched stress fibers. Myofibroblasts were transfected with GFP-actin and subsequently grown on bead micropatterned silicon rubber. Immediately before the experiment, lines approximately perpendicular to the direction of deformation (white arrow) were bleached into the GFP-labeled actin stress fibers (A). Edges of bleach lines in cortical stress fibers (upper fiber in indicated white box) were tracked by cross-correlation during substrate deformation. In order to compare stress fiber motion with substrate deformation, the displacements of all beads below analyzed stress fibers were determined. Displacements of the cortical stress fiber from the upper white box (green arrows) and of the underlying beads (red arrows) are given before (B) and at maximum stretch (C) application. Scale bar = 20 μm, substrate/stress fiber displacement arrow = 2 μm.

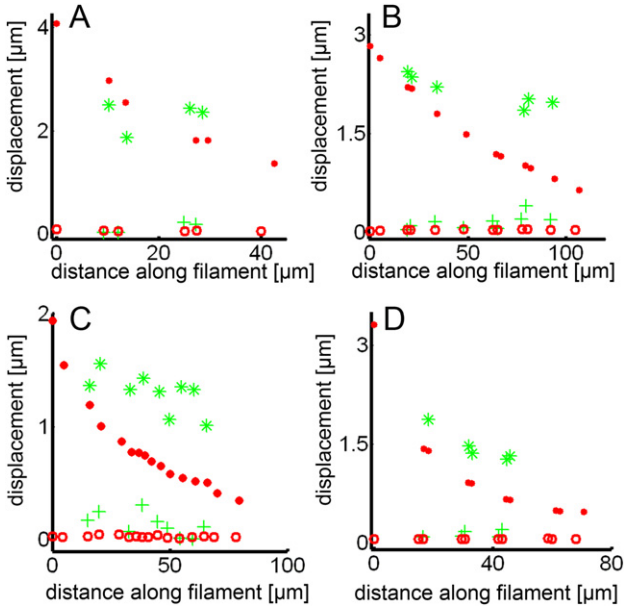

Figure 4. The major parts of stress fibers are stiff structures. Single cortical stress fibers of four independent cells (A–D) were labeled by bleached lines as given in figure 3. Subsequently, labels along stress fibers (green), as well as underlying fluorescent beads (red), were tracked before (cross and open circle) and at maximum substrate deformation (asterisks and closed circles). Note the decaying substrate deformation field while displacements along stress fibers exhibited a much weaker, approximately linear decay. $n = 10$ stress fibers from 8 independent cells. An error of 0.24 μm for GFP and 0.03 μm for bead signals (substrate) describes the system noise and therefore the tracking uncertainty. This was determined using the standard deviation of all GFP and bead displacements, respectively, over the whole time period before application of any substrate deformation.

3.3. Stress fibers move relative to focal adhesions

Up to now we found that only a minor fraction of the substrate displacement was balanced by a lengthening of the stress fiber. Moreover, mechanical integrity of the cell was retained. To identify the softest link in the mechanical system, the displacement of stress fibers relative to adhesion sites was analyzed in more detail. Myofibroblasts were simultaneously

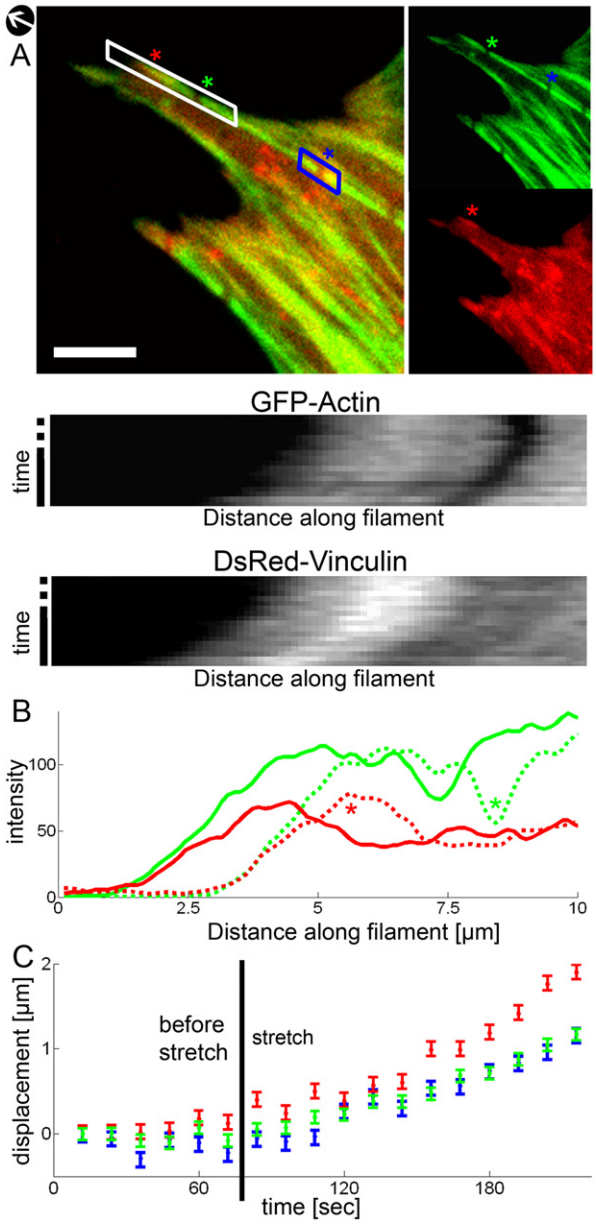

Figure 5. Distance between stress fiber ends and FAs increases during stretch. (A) Myofibroblasts were transfected with GFP-actin and DsRed-vinculin simultaneously. Before substrate deformation (white arrow) thin lines perpendicular to the substrate deformation were bleached into the stress fibers (green and blue asterisk). Upon substrate deformation, intensity profiles along the white box were determined for actin and vinculin. Both are indicated as time–space-plots with a time interval of 12 s. Scale bar = 20 μm. (B) Intensity profiles before (dashed lines) and at maximum substrate deformation (full line) are given for GFP-actin (green) and DsRed-vinculin (red). The red and the green star indicate maximum vinculin intensity and the center of the first actin bleach line, respectively. These positions, as well as the second bleach line (blue asterisk in A), were tracked for every substrate deformation step and their displacements were plotted (C). In this case the stress fiber displacements of both bleach lines represent approximately half the displacement of FA. The error given for each value describes the system noise and therefore the tracking uncertainty. The value represents the standard deviation of FA (0.074 μm) and actin bleach line (0.075 μm, green asterisk and 0.106 μm, blue asterisk) displacements, respectively, over the whole time period without application of any substrate deformation (approximately first 80 s). $n = 5$ independent experiments.

transfected with GFP-actin and DsRed-vinculin ($n = 5$ independent cells). Directly before the measurement actin fibers were labeled by thin bleached lines closely behind the FA site and additionally approximately 15 μm distance away (figure 5(A)). Subsequently, intensity profiles along the FA, as well as along the first actin bleach line, were continuously recorded and substrate deformation was induced. These profiles revealed before and at maximal substrate deformation strong displacements for FAs as well as for the stress fibers (figure 5(B)). Since substrate deformation was performed stepwise, the maximum of the vinculin intensity and the actin bleach line were tracked for each step of substrate deformation. While the displacement of the vinculin signal was high (figure 5(C)), resembling substrate deformation (not shown), actin stress fiber displacement was just a fraction of substrate/FA displacement leading to an increasing distance between FA and the first stress fiber bleach line. This behavior was independent of the deformation amplitude applied. Displacement analysis of the second actin bleach line at 15 μm distance from the FA revealed identical values as found for the first one. These results corroborate the rigid character of stress fibers under tensile strain, with an elongation only at their ends.

3.4. No actin polymerization takes place at stress fiber ends upon tensile strain

While FAs were found to be firmly connected to the substrate for all proteins analyzed here, substrate deformations are not fully transferred to actin stress fibers. This type of behavior could be explained by various mechanisms such as an elastic or plastic deformation of stress fiber ends or by actin polymerization induced by tensile strain. In a first step, a putative stress fiber elongation by actin polymerization upon substrate elongation was analyzed. Cells were transfected with GFP-actin (figure 6(A)) and stress fibers were labeled by bleached lines ($n = 5$). Since putative actin polymerization was supposed to take place at the end of stress fibers, single ends were additionally completely bleached directly before the start of the experiment (figure 6(B)). Neighboring stress fiber ends remained unbleached and served as an internal control. Upon whole stress fiber elongation by 2% no new appearance of GFP signals and therefore no induced actin polymerization were observed. Due to the relatively stiff character of inner stress fiber parts (see figure 4), the stress fibers serving as an internal control became elongated only at their ends. Hereby, the 2% whole stress fiber elongation resulted in an elongation of the stress fiber ends by almost 10%.

3.5. Cell specific substrate deformation fields remains similar during cell stretch

Depending on whether stress fiber ends undergo plastic or elastic deformation, elongated fiber ends could reduce traction forces and thus the corresponding substrate deformation fields after release of substrate deformation. For this reason we analyzed substrate deformation fields of cells transfected with GFP-actin and cultured on bead-microstructured silicone rubber ($n = 7$ independent cells). For all subsequent

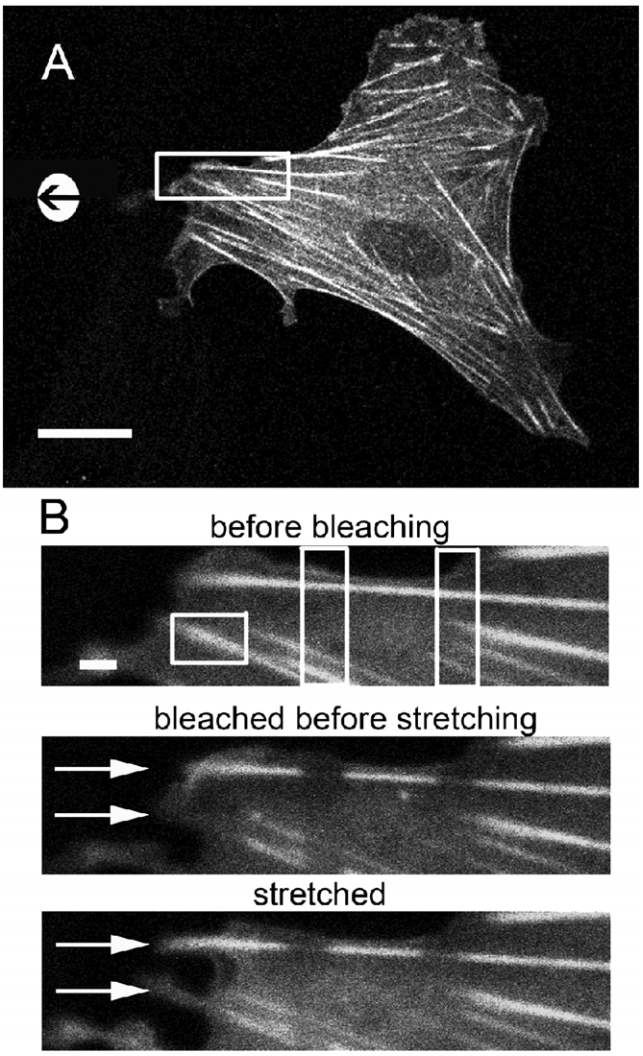

Figure 6. No actin polymerization is induced during substrate deformation. (A) GFP-actin expressing myofibroblasts were grown on elastomeric substrates. Scale bar = 20 μm. (B) Directly before substrate deformation (white dot and black arrow) stress fibers were marked by bleaching lines perpendicular to the direction of deformation. Additionally, one end of a single stress fiber was bleached completely (small rectangle, lower arrow). Subsequently substrate deformation was induced and GFP-actin signals analyzed over time. Stress fibers with only bleached stripes served as an internal control for the stability of the system. Note that at no time could new GFP-actin signals be observed at the end of the bleached stress fiber. Scale bar = 2 μm. $n = 5$ independent experiments.

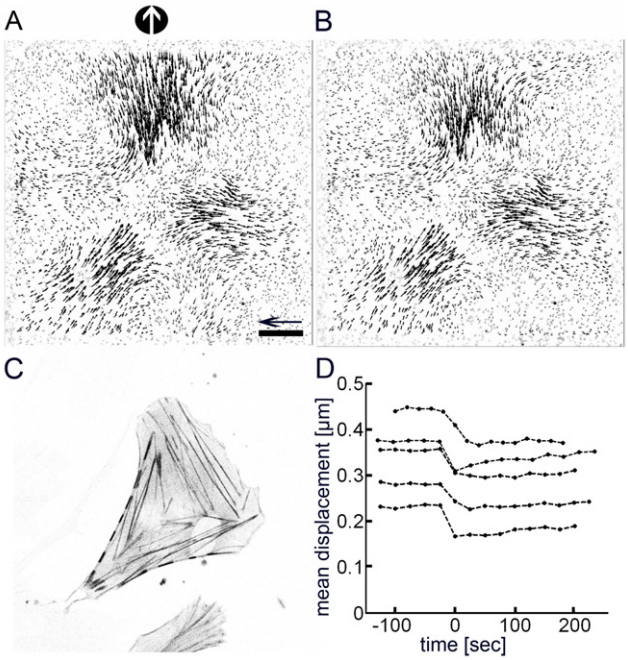

Figure 7. Substrate deformation fields remain largely stable after stretch application. (C) Myofibroblasts were transfected with GFP-actin and grown on elastic substrates. Directly before substrate deformation (white arrow) thin lines perpendicular to the substrate deformation were bleached into the stress fibers. Beads were tracked before and after microneedle induced substrate deformation. Subsequently, every analyzed cell was removed mechanically from the substrate and bead positions were determined to serve as a force free reference. This reference allowed the calculation of the cell specific substrate deformation field before (A) and after (B) external substrate deformation. This example (A–C) was also analyzed in figure 4(C). Calculated mean displacement values before and after substrate deformation are given in (D). Time point zero indicates mean displacement value directly after substrate deformation. Results were identical for untransfected cells and cells transfected with GFP versions of either actin, VASP or vinculin. In total: $n = 8$ independent cells. Scale bar = 20 μm. Arrow = 2 μm displacement.

analyses a reference image of the undeformed substrate at the location of every analyzed cell was needed and obtained by manual removal of the cell at the end of an analysis cycle. Comparing bead positions before (figure 7(A)) and after (figure 7(B)) application of a decaying deformation field to a cell with reference bead positions showed similar substrate deformation fields after a certain relaxation period. For more accurate substrate deformation analyses, mean substrate deformation values were compared. These were reduced by just 17% on average directly after stretch application. Mean substrate deformation values either stayed constant or even increased again to values close to those found before substrate stretch (figure 7(D)). We found largely similar mean substrate deformations before and after substrate stretch, also for cells expressing no or various other GFP constructs such as GFP-vinculin, or GFP-VASP. Simultaneous analysis of every cell in phase contrast or fluorescence (figure 7(C)) guaranteed that the overall cell morphology stayed unaffected upon substrate deformation. These data argue for a relatively stable force value applied by the cell to the substrate even when the FA/stress fiber system was elongated by an external deformation field.

3.6. Cell elongation results in a plastic deformation of stress fiber ends

The possibility of elastic or static deformation at stress fiber ends was analyzed in more detail since these parts were excluded from the analyses given in figure 4. Stress fibers of GFP-actin transfected cells were labeled by bleach lines and subsequently stretched by one complete stretch and release cycle. Release was performed by active return of

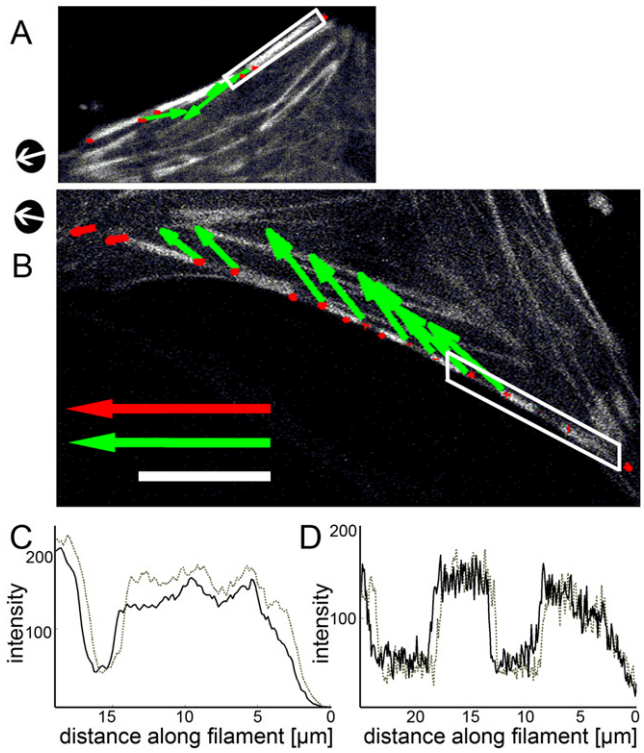

Figure 8. Plastic deformation of the stress fiber ends is compensated by inner stress fiber contraction. GFP-actin transfected myofibroblasts were handled as described in figure 4 and displacements of substrate beads (red arrows), as well as of bleached lines (green arrows), were tracked directly after release of substrate deformation ((A) and (B), representing two independent cells out of $n = 7$). Intensity profiles along the white boxes indicated in (A) and (B) are given ((C) and (D)) before (gray dotted line) and after (black line) substrate stretch. Note that the positions of the substrate beads as well as of the stress fiber ends are almost the same as before stretch application. After stretch, the stress fiber ends are elongated. In contrast, the inner parts of the stress fibers contract leading to displacements. Scale bar = 20 μm. Arrow = 2 μm displacement.

the microneedle to its original position in order to reduce putative viscoelastic relaxation, i.e. slow creeping back, of the substrate. This led to spatially nearly unaffected localizations of stress fiber ends (figures 8(C) and (D), minimal intensity at 0 μm). Analyzing distances from stress fiber ends to the first bleach line at 8–15 μm distances we found significant elongations of these areas upon substrate stretch, as already shown before. Interestingly, this increased length from the stress fiber ends to the first bleach line also remained stable after stretch release (figures 8(C) and (D), dotted line). Elongation values varied, since the two ends of a single actin fiber elongated differently, most likely elongating more on the weaker site ($n = 7$ independent stress fibers). Same analyses 3 min after stretch revealed identical results (not shown), strongly arguing for a plastic deformation of the stress fiber ends. While the stress fiber ends were plastically elongated, opposite results were found for the inner parts of stress fibers. Here, stress fibers started to contract after substrate release. This contraction resulted in an inwardly directed displacement of the bleached lines (figures 8(A) and (B)). Displacements were directed either to the center of stress fibers, when both ends were elongated by similar values (figure 8(A)), or displaced in the direction of the stiffer stress fiber end (figure 8(B)). The data therefore argue that the interplay between plastic deformation of the stress fiber ends and subsequent contraction of the inner fiber leaves the cell tension largely unaffected.

4. Discussion

In this project we aimed at identifying the weakest link in the mechanical connections between the cellular environment and the actin stress fibers. This weakest linkage is also the location of most intense relative motion between, and within, proteins and thus a likely location for mechanosensitive proteins. We therefore developed an experimental setup in which the substrate, focal adhesions as well as the actin fibers could be permanently analyzed before, during, and after application of localized deformation fields. Since most of the protein interactions were supposed to be stiff, small elongations of the systems were assumed to have significant and detectable effects in deformable parts of the mechanical chains. Due to active cell traction forces, the whole stress fiber-adhesion apparatus was furthermore under pre-tension, which should enhance its sensitivity for applied mechanical signals. In our case we applied substrate stretches in the range from 1 to 3% below the cell. These amplitudes were sufficient for detection of cell compartments that were deformed by the concomitant stresses, but small enough to prevent large scale or even artificial cell behavior such as release of adhesion or induction of cell reorientation. Furthermore, substrate deformation fields were applied to a localized area of the cell, keeping overall stress levels as low as possible. Measurement of applied forces by traction force microscopy could not be performed since the contact area of the microneedle, and especially its indentation into the substrate during elastomer deformation, could not be quantified well.

As already mentioned above, our system strongly depends on the high temporal stability of focal adhesion sites and stress fibers. We therefore chose differentiated myofibroblasts as the model system since these cells were known to have cytoskeletal and adhesion structures spatially stable over hours [45], which by far exceeds the duration of our experiments (below 10 min). Lamellipodial dynamics, formation of new adhesion sites or spontaneous cell form alterations were rarely detectable. Furthermore, myofibroblasts apply significant traction forces keeping the cytoskeletal–adhesion system well tensed. For this cellular system we could identify a rigid connection between all analyzed focal adhesion proteins and the substrate. With an accuracy of 50 nm for fluorescent bead tracking (substrate) and 100 nm for focal adhesion sites, all FA proteins tested revealed identical displacements to the underlying substrate in decaying deformation fields. We cannot exclude small deformations below the detection limit within FAs or at the contact site to the substrate. Nevertheless, with a small level of uncertainty we conclude that almost all substrate deformation was transferred to the stress fibers adhered to FAs. This finding allows an interesting extension to results found in cell types characterized by a faster dynamics. There, focal adhesion proteins show an

increased mobility in the direction of actin retrograde flow the closer proteins are connected to attached actin filaments [42]. Traction forces on their own can therefore already result in an elongation of FAs even without application of external force fields. However, protein composition [46], exchange dynamics as well as phosphorylation patterns [47] and the response to external force application [4–6] are known to be different between dynamic and mature FAs. It is therefore likely that both types of FAs are characterized by different mechanical properties.

Since stress fibers are long and mostly homogeneous structures, accurate analysis of stress fiber elongation upon external stress field application made the division of every fiber into distinct sections necessary. Photobleaching of GFP-actin labeled actin fibers was chosen, since neither expression of actin fusion proteins nor photobleaching itself induced artificial cell behavior. To analyze stress fiber displacement in the most unaffected environment, we typically chose separated fibers at the cell cortex with only one adhesion site at each end [48]. Stress fibers not fulfilling these criteria could hardly be analyzed since their displacements showed large variations. Stretching inner stress fibers we observed propagation of the fiber displacements to other visibly connected or neighboring fibers. The high diversity of the stress fiber network within these cells caused the observed high variability of the results on such inner fibers; these were therefore excluded from further analysis.

Our results separate every stress fiber into two distinct sections. The first one comprises almost the whole fiber except its ends. This part is comparably stiff upon cell elongation. As result, the whole inner section was displaced by almost constant values. This finding fits well to former results describing stress fibers as non-extendable structures [11, 39]. The second section covers both stress fiber ends. Here, pronounced elongations could be observed upon cell extension. Interestingly, both ends of identical stress fibers were not necessarily elongated by identical values. In fact, most often one end region was elongated significantly more than the other. This argues for an efficient transfer of mechanical force over the whole stress fiber and a more prominent elongation at the weaker adhesion site. Exact determination of elongation values often turned out to be difficult since elongation did not go along with new actin polymerization. This led to blurred actin signals of reduced intensity at their connections to FAs. These signals were often close to background levels and, therefore, were often lost during image processing routines. Although not analyzed in this work, others could prove a changing protein composition along stress fibers [37]. While cross-linker proteins such as α-actinin or zyxin are localized mainly at the ends of stress fibers, myosin II is incorporated in the inner part with a distinct distance from the stress fiber ends. We can only speculate whether these proteins are also responsible for the changing elasticity behavior of stress fibers along their axis, as found here. Nevertheless, a modified protein pattern will most likely be responsible for this effect, since the number of actin filaments stays relatively constant along the whole length of stress fibers [37, 49].

The stress fiber behavior upon release of substrate deformation was surprising to us. Here, we could show that elongated stress fiber ends were plastically deformed, keeping their extended lengths. Even prolonged analysis times after release showed barely any recovery. In contrast, the excess of total stress fiber length was compensated by the contraction of the inner stress fiber sections over time. This behavior led to almost unaffected substrate deformation fields after release, arguing that transmitted traction force values were unaffected. In addition, small reductions directly after release were partly compensated within a few minutes (see figure 7).

In total, we propose the important biological relevance of the linkage between stress fibers and adhesions based on their mechanical properties identified in this work. The data indicate that mechanosensitive proteins of sessile cells will be affected by mechanical signals most efficiently if incorporated into stress fiber ends, while FAs themselves are structures relatively stiff against cell extension. The plastic, i.e. persistent, deformation of stress fiber ends further implies that mechanotransduction processes could already be induced by single mechanical events. Frequent repetition of signal application might therefore be of minor importance. We further propose that traction forces, vital for cell function and morphology, can be kept stable upon mechanosensation and transduction. This might be a reason why myosin II is not located at stress fiber ends, leaving an elongation and putative conformational change of embedded molecules unaffected.

Acknowledgment

We thank I Lauter, M Giesen and C Möhl for helpful discussions and critical reading of the manuscript. We are grateful to W Rubner for intense technical support. The GFP-vinculin construct was kindly provided by B Geiger (Weizmann Institute of Science, Israel). The GFP-VASP plasmid was a kind gift from J Wehland (University Braunschweig, Germany).

References

[1] Kaunas R, Nguyen P, Usami S and Chien S 2005 Cooperative effects of Rho and mechanical stretch on stress fiber organization *Proc. Natl Acad. Sci. USA* **102** 15895–900

[2] Hayakawa K, Sato N and Obinata T 2001 Dynamic reorientation of cultured cells and stress fibers under mechanical stress from periodic stretching *Exp. Cell. Res.* **268** 104–14

[3] Bershadsky A D, Balaban N Q and Geiger B 2003 Adhesion-dependent cell mechanosensitivity *Annu. Rev. Cell. Dev. Biol.* **19** 677–95

[4] Riveline D *et al* 2001 Focal contacts as mechanosensors: externally applied local mechanical force induces growth of focal contacts by an mDia1-dependent and ROCK-independent mechanism *J. Cell. Biol.* **153** 1175–86

[5] Paul R, Heil P, Spatz J P and Schwarz U S 2008 Propagation of mechanical stress through the actin cytoskeleton toward focal adhesions: model and experiment *Biophys. J.* **94** 1470–82

[6] Galbraith C G, Yamada K M and Sheetz M P 2002 The relationship between force and focal complex development *J. Cell. Biol.* **159** 695–705

[7] Walter N, Selhuber C, Kessler H and Spatz J P 2006 Cellular unbinding forces of initial adhesion processes on nanopatterned surfaces probed with magnetic tweezers *Nano Lett.* **6** 398–402
[8] Goffin J M, Pittet P, Csucs G, Lussi J W, Meister J J and Hinz B 2006 Focal adhesion size controls tension-dependent recruitment of alpha-smooth muscle actin to stress fibers *J. Cell. Biol.* **172** 259–68
[9] Solon J, Levental I, Sengupta K, Georges P C and Janmey P A 2007 Fibroblast adaptation and stiffness matching to soft elastic substrates *Biophys. J.* **93** 4453–61
[10] Engler A J, Sen S, Sweeney H L and Discher D E 2006 Matrix elasticity directs stem cell lineage specification *Cell* **126** 677–89
[11] Deguchi S and Sato M 2009 Biomechanical properties of actin stress fibers of non-motile cells *Biorheology* **46** 93–105
[12] Zamir E and Geiger B 2001 Molecular complexity and dynamics of cell-matrix adhesions *J. Cell. Sci.* **114** 3583–90 (Pt 20)
[13] Pellegrin S and Mellor H 2007 Actin stress fibres *J. Cell. Sci.* **120** 3491–9 (Pt 20)
[14] Peterson L J, Rajfur Z, Maddox A S, Freel C D, Chen Y and Edlund M *et al* 2004 Simultaneous stretching and contraction of stress fibers *in vivo Mol. Biol. Cell.* **15** 3497–508
[15] Geiger B, Spatz J P and Bershadsky A D 2009 Environmental sensing through focal adhesions *Nat. Rev. Mol. Cell. Biol.* **10** 21–33
[16] Wang H B, Dembo M, Hanks S K and Wang Y 2001 Focal adhesion kinase is involved in mechanosensing during fibroblast migration *Proc. Natl Acad. Sci. USA* **98** 11295–300
[17] Hinz B, Mastrangelo D, Iselin C E, Chaponnier C and Gabbiani G 2001 Mechanical tension controls granulation tissue contractile activity and myofibroblast differentiation *Am. J. Pathol.* **159** 1009–20
[18] Gabbiani G 2003 The myofibroblast in wound healing and fibrocontractive diseases *J. Pathol.* **200** 500–3
[19] McCue S, Noria S and Langille B L 2004 Shear-induced reorganization of endothelial cell cytoskeleton and adhesion complexes *Trends Cardiovasc. Med.* **14** 143–51
[20] Discher D E, Janmey P and Wang Y L 2005 Tissue cells feel and respond to the stiffness of their substrate *Science* **310** 1139–43
[21] Engler A J, Griffin M A, Sen S, Bonnemann C G, Sweeney H L and Discher D E 2004 Myotubes differentiate optimally on substrates with tissue-like stiffness: pathological implications for soft or stiff microenvironments *J. Cell. Biol.* **166** 877–87
[22] Engler A J, Sen S, Sweeney H L and Discher D E 2006 Matrix elasticity directs stem cell lineage specification *Cell* **126** 677–89
[23] Wang J H, Goldschmidt-Clermont P, Wille J and Yin F C 2001 Specificity of endothelial cell reorientation in response to cyclic mechanical stretching *J. Biomech.* **34** 1563–72
[24] Chen C S, Mrksich M, Huang S, Whitesides G M and Ingber D E 1997 Geometric control of cell life and death *Science* **276** 1425–8
[25] Thery M, Pepin A, Dressaire E, Chen Y and Bornens M 2006 Cell distribution of stress fibres in response to the geometry of the adhesive environment *Cell. Motil. Cytoskeleton* **63** 341–55
[26] Flemming R G, Murphy C J, Abrams G A, Goodman S L and Nealey P F 1999 Effects of synthetic micro- and nano-structured surfaces on cell behavior *Biomaterials* **20** 573–88
[27] Lim J Y and Donahue H J 2007 Cell sensing and response to micro- and nanostructured surfaces produced by chemical and topographic patterning *Tissue Eng.* **13** 1879–91
[28] Vogel V and Sheetz M 2006 Local force and geometry sensing regulate cell functions *Nat. Rev. Mol. Cell. Biol.* **7** 265–75
[29] Krammer A, Lu H, Isralewitz B, Schulten K and Vogel V 1999 Forced unfolding of the fibronectin type III module reveals a tensile molecular recognition switch *Proc. Natl Acad. Sci. USA* **96** 1351–6
[30] Kung C 2005 A possible unifying principle for mechanosensation *Nature* **436** 647–54
[31] Thomas W E, Trintchina E, Forero M, Vogel V and Sokurenko E V 2002 Bacterial adhesion to target cells enhanced by shear force *Cell* **109** 913–23
[32] Wei C, Wang X, Chen M, Ouyang K, Song L S and Cheng H 2009 Calcium flickers steer cell migration *Nature* **457** 901–5
[33] Bruinsma R 2005 Theory of force regulation by nascent adhesion sites *Biophys. J.* **89** 87–94
[34] Nicolas A, Geiger B and Safran S A 2004 Cell mechanosensitivity controls the anisotropy of focal adhesions *Proc. Natl Acad. Sci. USA* **101** 12520–5
[35] Shemesh T, Otomo T, Rosen M K, Bershadsky A D and Kozlov M M 2005 A novel mechanism of actin filament processive capping by formin: solution of the rotation paradox *J. Cell. Biol.* **170** 889–93
[36] Sawada Y *et al* 2006 Force sensing by mechanical extension of the Src family kinase substrate p130Cas *Cell* **127** 1015–26
[37] Colombelli J *et al* 2009 Mechanosensing in actin stress fibers revealed by a close correlation between force and protein localization *J. Cell. Sci.* **122** 1665–79
[38] Yoshigi M, Hoffman L M, Jensen C C, Yost H J and Beckerle M C 2005 Mechanical force mobilizes zyxin from focal adhesions to actin filaments and regulates cytoskeletal reinforcement *J. Cell. Biol.* **171** 209–15
[39] Bischofs I B, Klein F, Lehnert D, Bastmeyer M and Schwarz U S 2008 Filamentous network mechanics and active contractility determine cell and tissue shape *Biophys. J.* **95** 3488–96
[40] Deguchi S, Ohashi T and Sato M 2005 Intracellular stress transmission through actin stress fiber network in adherent vascular cells *Mol. Cell. Biomech.* **2** 205–16
[41] Kumar S *et al* 2006 Viscoelastic retraction of single living stress fibers and its impact on cell shape, cytoskeletal organization, and extracellular matrix mechanics *Biophys. J.* **90** 3762–73
[42] Hu K, Ji L, Applegate K T, Danuser G and Waterman-Storer C M 2007 Differential transmission of actin motion within focal adhesions *Science* **315** 11–5
[43] Merkel R, Kirchgessner N, Cesa C M and Hoffmann B 2007 Cell force microscopy on elastic layers of finite thickness *Biophys. J.* **93** 3314–23
[44] Cesa C M, Kirchgessner N, Mayer D, Schwarz U S, Hoffmann B and Merkel R 2007 Micropatterned silicone elastomer substrates for high resolution analysis of cellular force patterns *Rev. Sci. Instrum.* **78** 034301
[45] Hinz B, Phan S H, Thannickal V J, Galli A, Bochaton-Piallat M L and Gabbiani G 2007 The myofibroblast: one function, multiple origins *Am. J. Pathol.* **170** 1807–16
[46] Zaidel-Bar R, Cohen M, Addadi L and Geiger B 2004 Hierarchical assembly of cell-matrix adhesion complexes *Biochem. Soc. Trans.* **32** 416–20
[47] Möhl C *et al* 2009 Becoming stable and strong: the interplay between vinculin exchange dynamics and adhesion strength during adhesion site maturation *Cell. Motil. Cytoskeleton* **66** 350–64
[48] Zand M S and Albrecht-Buehler G 1989 What structures, besides adhesions, prevent spread cells from rounding up? *Cell. Motil. Cytoskeleton* **13** 195–211
[49] Cramer L P, Siebert M and Mitchison T J 1997 Identification of novel graded polarity actin filament bundles in locomoting heart fibroblasts: implications for the generation of motile force *J. Cell. Biol.* **136** 1287–305